

Fermi GBM Observations of LIGO Gravitational Wave event GW150914

V. Connaughton^{*,1}, E. Burns², A. Goldstein^{+,3}, M. S. Briggs⁴, B.-B. Zhang⁵, C. M. Hui³,
 P. Jenke⁵, J. Racusin⁶, C. A. Wilson-Hodge³, P. N. Bhat⁵, E. Bissaldi⁷, W. Cleveland¹,
 G. Fitzpatrick⁵, M. M. Giles⁸, M. H. Gibby⁸, J. Greiner⁹, A. von Kienlin⁹, R. M. Kippen¹⁰,
 S. McBreen¹¹, B. Mailyan⁵, C. A. Meegan⁵, W. S. Paciesas¹, R. D. Preece⁴, O. Roberts¹⁰,
 L. Sparke¹², M. Stanbro², K. Toelge⁹, P. Veres⁵, H.-F. Yu^{9,13}

and other authors

ABSTRACT

With an instantaneous view of 70% of the sky, the *Fermi* Gamma-ray Burst Monitor (GBM) is an excellent partner in the search for electromagnetic counterparts to gravitational wave (GW) events. GBM observations at the time of the Laser Interferometer Gravitational-wave Observatory (LIGO) event GW150914 reveal the presence of a weak transient source above 50 keV, 0.4 s after the GW event was detected, with a false alarm probability of 0.0022. This weak transient lasting 1 s does not appear connected with other previously known astrophysical, solar, terrestrial, or magnetospheric activity. Its localization is ill-constrained but consistent with the direction of GW150914. The duration and spectrum of the transient event suggest it is a weak short Gamma-Ray Burst arriving at a large angle to the direction in which *Fermi* was pointing, where the GBM

*Email: valerie@nasa.gov

⁺NASA Postdoctoral Fellow

¹Universities Space Research Association, 320 Sparkman Dr. Huntsville, AL 35806, USA

²Physics Dept, University of Alabama in Huntsville, 320 Sparkman Dr., Huntsville, AL 35899, USA

³Astrophysics Office, ZP12, NASA/Marshall Space Flight Center, Huntsville, AL 35812, USA

⁴Dept. of Space Science, University of Alabama in Huntsville, 320 Sparkman Dr., Huntsville, AL 35899, USA

⁵CSPAR, University of Alabama in Huntsville, 320 Sparkman Dr., Huntsville, AL 35899, USA

⁶NASA Goddard Space Flight Center, Greenbelt, MD 20771, USA

⁷Istituto Nazionale di Fisica Nucleare, Sezione di Bari, 70126 Bari, Italy

⁸Jacobs Technology, Inc., Huntsville, AL, USA

⁹Max-Planck-Institut für extraterrestrische Physik, Giessenbachstrasse 1, 85748 Garching, Germany

¹⁰Los Alamos National Laboratory, NM 87545, USA

¹¹School of Physics, University College Dublin, Belfield, Stillorgan Road, Dublin 4, Ireland

¹²NASA Headquarters, Washington DC, USA

¹³Excellence Cluster Universe, Technische Universität München, Boltzmannstr. 2, 85748, Garching, Germany

detector response is not optimal. If the GBM transient is associated with GW150914, this electromagnetic signal from a stellar mass black hole binary merger is unexpected. From our measurement of the fluence seen by GBM, we calculate a luminosity in hard X-ray emission between 1 keV and 10 MeV of $1.8_{-1.0}^{+1.5} \times 10^{49}$ erg s⁻¹. The observation by *Fermi* GBM encompasses 75% of the probability map associated with the LIGO GW event localization at the time the GW event was detected. Assuming the two events have a common origin, the combined LIGO and GBM observations can reduce the 90% confidence interval on sky location from 601 to 199 square degrees. Future joint observations of GW events by LIGO/Virgo and *Fermi* GBM could reveal whether the weak transient reported here is a plausible counterpart to the GW event GW150914 or a chance coincidence, and will further probe the connection between compact binary mergers and short Gamma-Ray Bursts.

1. Introduction

The Gamma-ray Burst Monitor (GBM) on the *Fermi* Gamma-ray Space Telescope is an all-sky hard-X-ray monitor that is ideally suited to detect rare and unpredictable transient events. Since the launch of *Fermi* in June 2008, GBM has triggered on-board nearly 5000 times in response to short-lived impulsive bursts lasting from under a millisecond to hundreds of seconds. This collection of triggered events¹ includes nearly 1800 Gamma-Ray Bursts (GRBs; von Kienlin et al. (2014)), 1100 solar flares, 200 bursts from 9 separate magnetars, and over 600 Terrestrial Gamma-ray Flashes (TGFs). Dedicated offline searches over all or parts of the mission have yielded over 200 additional magnetar bursts (Collazzi et al. 2015), thousands of additional TGFs² (Briggs et al. 2013), nearly 700 type I thermonuclear bursts from galactic binary systems (Jenke et al. 2016), non-impulsive steady or variable emission from over 100 mostly galactic sources (Wilson-Hodge et al. 2012)³, and pulsed emission from 35 accretion-powered galactic binary systems⁴.

Detection of gravitational waves (GW) reported by Laser Interferometer Gravitational-wave Observatory (LIGO; LIGO Scientific Collaboration et al. (2015)) and Virgo experiment (Acernese et al. 2015) has been eagerly anticipated. LIGO/Virgo are sensitive to the GW from mergers of stellar mass compact objects in a binary system as well as other sources. The most promising electromagnetic counterpart to a compact binary merger involving a neutron star is a short GRB, although the joint GW-GRB detection rate is expected to be low given the collimation of the GRB emission (both prompt and afterglow radiation) and the detection horizons of LIGO/Virgo

¹<http://heasarc.gsfc.nasa.gov/W3Browse/fermi/fermigtrig.html>

²<http://fermi.gsfc.nasa.gov/ssc/data/access/gbm/tgf/>

³<http://heastro.phys.lsu.edu/gbm/>

⁴<http://gammaray.nsstc.nasa.gov/gbm/science/pulsars.html>

(Siellez et al. 2014) for these progenitors. Although other electromagnetic counterparts have been suggested, notably r-process transients produced in the ejecta resulting from the binary merger (Metzger et al. 2010), only one such event has been reported (Tanvir et al. 2013; Berger et al. 2013), compared to 300 short GRBs detected by GBM, a rate of ~ 40 per year (von Kienlin et al. 2014). With the implementation in 2015 of an offline search of the GBM data, the rate of short GRBs detected by GBM may be increased to ~ 80 per year. Validating these additional short GRB candidates and refining the search criteria will allow the GBM team to deploy an efficient pipeline for the identification and communication in near real-time of sub-threshold short GRBs during upcoming observing runs of the LIGO and Virgo experiments.

In addition to this offline untargeted search of the GBM data, we developed targeted searches and efficient data analysis pipelines to identify electromagnetic counterparts to any candidate GW events in the GBM data. Joint localization of these events will improve the localizations done separately, which will assist follow-up observers using pointed instruments to identify the host galaxy and thus the redshift of the source. We exercised and refined these pipelines during Advanced LIGO’s summer 2015 engineering runs in preparation for the first Advanced LIGO observing run (O1). On 2015 September 16, the LIGO and Virgo collaborations reported that a candidate event, G184098, had been identified in data recorded on September 14 (The LIGO Scientific Collaboration and Virgo 2015a; Abbott et al. 2016)⁵. The candidate was subsequently characterized as being consistent with a signal from the merger of a stellar mass black hole binary system (The LIGO Scientific Collaboration and Virgo 2015b), with a false alarm rate of less than one per century (The LIGO Scientific Collaboration and Virgo 2015c), and was announced publicly in Abbott et al. (2016) as GW event GW150914. Although there are no predictions or well-established mechanisms for detectable EM emission from stellar mass binary black hole mergers to guide a search for counterparts in the GBM data, we carried out a methodical search around the time and sky location of the event GW150914, which we report in the following section.

2. GBM Observations of GW150914

GBM consists of 12 Thallium-doped Sodium Iodide (NaI) detectors with a diameter of 12.7 cm and a thickness of 1.27 cm and two Bismuth Germanate (BGO) detectors with a diameter and thickness of 12.7 cm (Meegan et al. 2009). The NaI detectors are sensitive between 8 keV and 1 MeV and the BGO detectors extend the energy range to 40 MeV. The GBM flight software was designed so that GBM can trigger on-board in response to impulsive events, when the count rates recorded in two or more NaI detectors significantly exceed the background count rate on at least

⁵Information about GW event candidates and follow-up observations was exchanged in Gamma-ray Coordinates Network (GCN) Notices and Circulars which initially were restricted to groups which had established agreements with LIGO and Virgo. The Circulars regarding G184098 will be added to the public archive when the details of GW150914 are published.

one time-scale from 16 ms to 4.096 s in at least one of three energy ranges above 50 keV. Strong background variations below 50 keV hinder the simple background fitting needed for automated operation on the spacecraft. On short time-scales, the variations are less significant and triggering can be enabled in the 25 – 50 keV range on time-scales below 128 ms, resulting in the on-board detection of 200 magnetar bursts. GBM data can be probed at the longer time-scales and lower energy ranges in offline searches dedicated to particular objects, including type I thermonuclear bursts (Jenke et al. 2016) and additional, weaker magnetar bursts (Collazzi et al. 2015). The modification of the GBM flight software to include data from the BGO detectors in the 16 ms triggering window has made GBM very sensitive to spectrally harder events associated with the electric fields in thunderstorms, Terrestrial Gamma-ray Flashes (Briggs et al. 2013).

GBM has an instantaneous sky coverage of about 70%, with the remainder blocked by the Earth. GBM operates continuously except when detector high voltages are turned off during passages of the *Fermi* spacecraft through regions of high particle precipitation activity in the South Atlantic Anomaly (SAA), $\sim 15\%$ of the time depending on where *Fermi* is in the 50-day precession cycle of its orbit. GBM was recording data (i.e., not in the SAA) continuously from nearly 2 hours before to over 7 hours after the GW event. Figure 1 shows the LIGO sky map from Abbott et al. (2016) with the shaded region indicating the region of sky occulted to *Fermi* by the Earth at the time of detection of the GW event. GBM observed 75% of the probability region in the location map during the detection of GW150914, with the full region becoming visible 25 minutes later.

GBM did not record any on-board triggers around the time of the GW detection, at 09:50:45.391 UT on 2015 September 14. The triggers closest in time were from two events on 2015 September 14 that are consistent with particle precipitation in or near the spacecraft, at 04:09:23 UT on entering the SAA, and at 14:21:34 UT, when *Fermi* was at high geomagnetic latitude, nearly 6 hours before and 4.5 hours after the GW event, respectively. GBM recorded triggers at similar points in the *Fermi* orbit on the preceding and following days, leaving no doubt as to their magnetospheric origin. These two triggered events were sufficiently far removed in time from GW150914 that GBM was operating in a nominal configuration in which it could have triggered on significant transient sources above the on-board threshold.

2.1. Detection and significance of weak, hard X-ray event GW150914-GBM

An offline search of the GBM Continuous Time-Tagged Event (CTTE) data for impulsive events too weak to trigger on-board *Fermi*, or from a sky position unfavorable to the two-detector on-board triggering requirement was implemented in 2015. The main motivation for this offline search was to increase the sensitivity of GBM to short GRBs during the period in which *Fermi*, LIGO, and Virgo operate jointly. The offline search currently operates on CTTE data from the 12 NaI detectors over four energy bands and 10 time-scales from 0.1 to 2.8 s, with multiple detection thresholds such that the joint chance probability of the signals in all detectors exceeding background levels above the lowest threshold level is 10^{-6} in one day. We estimate this improves sensitivity to

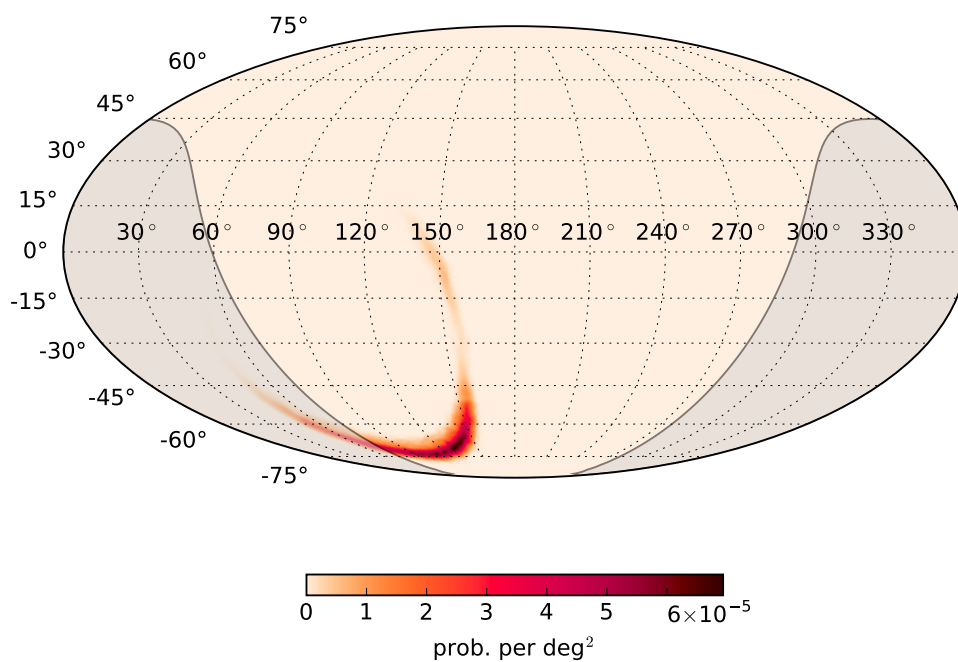


Fig. 1.— Localization map for GW150914, the GW event reported in Abbott et al. (2016). The grey shaded region indicates the region of sky occulted to *Fermi* by the Earth at the time of GW150914. The region not occulted by the Earth contains 75% of the probability of the localization map, with all but 6% of the probability contained in the lower lobe. The entire region was visible to *Fermi* GBM 25 minutes after the GW event was detected.

short GRBs by a factor of 2 – 3 in burst count fluence and the offline search detection rate of 1 – 4 candidate short GRBs per month is consistent with this estimate. The offline search reports no candidates above detection threshold on the day of the GW event⁶.

In addition to the undirected offline search, a targeted search of the GBM data was developed during S6, the last observing run of the previous configuration of LIGO (Blackburn et al. 2015a). By searching both GW and GBM datasets, the significance of a sub-threshold signal in one can be strengthened by the detection of a signal in the other, provided the false positive rate is manageable and well understood. It is estimated that the horizon of LIGO/Virgo can be boosted by 15 – 20% through this validation of sub-threshold candidates (Blackburn et al. 2015a; Kelley et al. 2013). The directed search of the GBM data is seeded with the time and (optionally) the sky location of any LIGO candidate event. A coherent search over all GBM detectors (NaI and BGO) using the full instrument response at each sky position is performed over a user-specified time window, revealing short-duration candidates typically between 0.256 s to 2 s in duration and ranked by a Bayesian likelihood statistic.

The technique was developed prior to the availability of CTTE data, using CTIME data, which are natively binned in 0.256 s accumulations with counts binned in 8 energy channels. The search has now been adapted to the 2 μ s unbinned CTTE data, providing much-improved sensitivity to very short bursts. While scanning trial foreground intervals for plausible bursts, the smoothly-varying GBM background in each detector is evaluated over time by a polynomial fit to nearby data on either side. This simple model is effective at characterizing the background behavior up to tens of seconds, effectively limiting the maximum duration of bursts that can be identified to a few seconds of local excess. Background-subtracted counts are then evaluated according to a likelihood-ratio statistic, comparing excesses due to Gaussian fluctuations with those arising from a modeled source with a particular amplitude, spectrum, and sky location. For the location, the model spectra are those used in the standard GBM source localization process (Connaughton et al. 2015), with three spectra parameterized by the Band function (Band et al. 1993) spanning the range of astrophysical phenomena we expect to uncover. A response to galactic transients, solar flares, and soft GRBs is expected to favor a soft spectrum. Long GRBs are typically best fit with an average spectrum, and a hard spectrum is often preferred for short GRBs. The Band function parameters for these three spectra are $\alpha, \beta, E_{peak} = (-1.9, -3.7, 70 \text{ keV}), (-1, -2.3, 230 \text{ keV}),$ and $(0, -1.5, 1 \text{ MeV}),$ respectively. The response to each spectrum is evaluated over all sky locations with an option to use a known source position as a prior in the evaluation of the likelihood. The events, characterized by their time and duration, are ranked by their likelihood ratios after marginalizing over their unknown source amplitude, spectrum, and sky position.

We searched 30 seconds of GBM data before and after the LIGO coalescence time for a plausible counterpart with duration between 0.256 s and 2 s. The ± 30 s interval we use is roughly guided by observation: if GRBs are related to compact binary mergers we expect the impulsive gamma-ray

⁶http://gammaray.nsstc.nasa.gov/gbm/science/sgrb_search.html

emission to be close in time to the GW, suggesting an interval of just a few seconds for our search. Precursors to short GRBs have, however, been observed farther than ~ 10 s prior to the main emission (Koshut et al. 1995; Burlon et al. 2009; Troja et al. 2010), and may originate from a less collimated emission region that is observable even when the GRB jet is not along the line-of-sight to the detector.

An all-sky search of the GBM data revealed two candidates. One transient, occurring at 09:50:56.8, 11 s after GW150914, was visible only below 50 keV, favored the soft model spectrum, and lasted 2 seconds. Using the standard GBM localization procedure we found a source position of RA, Dec = 267.7, -22.4 degrees, with a statistical uncertainty region of radius 15° . At a position in Galactic coordinates of $l, b = 6.2, 2.4$ degrees, the event is compatible with an origin near the galactic center, well separated from the LIGO localization region. It is typical of the type of soft X-ray transient activity seen regularly in the GBM background data. We do not view this transient event as being possibly related to GW150914 and we will not discuss it further.

The search also identified a hard transient which began at 09:50:45.8, about 0.4 s after the reported LIGO burst trigger time of 09:50:45.39, and lasted for about 1 second. The detector counts best matched those predicted from a hard model spectrum. We reported this event in Blackburn et al. (2015b); we henceforth call it GW150914-GBM. Figure 2 shows the model-dependent lightcurve of GW150914-GBM, where the detector data have been summed using weights that maximize signal-to-noise for a given source model, and the unknown source model itself is weighted according to its likelihood in the data.

2.2. The rate of detection of short hard transients in the GBM data

We use our targeted search to examine 240 ks of GBM data from September 2015 with 218822.1 s of GBM live-time, excluding passages of *Fermi* through or close to the SAA where the detectors are turned off or count rate increases overwhelm any attempt to fit a reasonable background model. We find 27 hard events with a higher log likelihood ratio than GW150914-GBM, corresponding to a rate of 1.23×10^{-4} Hz. This gives a 90% upper limit on the expected background of hard transients of 34.96, or 1.60×10^{-4} Hz. With a trials factor of 3 for the spectra, which were treated independently owing to their very different distributions, we obtain a false alarm rate of 4.79×10^{-4} Hz.

We determine the significance of a GBM counterpart candidate by considering both its frequency of occurrence, and its proximity to the GW trigger time. The candidates are assigned a false-alarm probability of $2\lambda\Delta t$ where λ is the candidate’s false-alarm rate in the GBM data, and Δt is its absolute time-difference to the GW time. Our method, described in Blackburn (2015)⁷ allows us to account for all the search windows in the interval over which we performed our search,

⁷<https://dcc.ligo.org/LIGO-T1500534/public>

GBM detectors at 150914 09:50:45.797 +1.024s

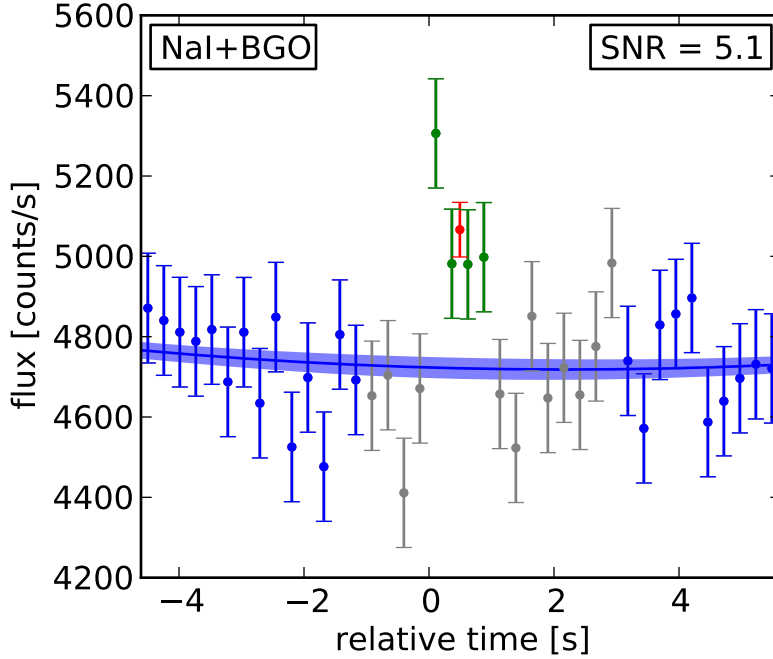


Fig. 2.— Count rates detected as a function of time relative to the start of GW150914-GBM, ~ 0.4 s after the GW event GW150914, weighted and summed to maximize signal-to-noise for a modeled source. CTIME time bins are 0.256 s wide. The blue data points are used in the background fit. The green points are the counts in the time period determined to be significant, the grey points are outside this time period, and the red points show the 1.024 s average over the green points. For a single spectrum and sky location, detector counts for each energy channel are weighted according to the modeled rate and inverse noise variance due to background. The weighted counts from all NaI and BGO detectors are then summed to obtain a signal-to-noise optimized light curve for that model. Each model is also assigned a likelihood by the targeted search based on the foreground counts (in the region of time spanned by the green points), and this is used to marginalize the light curve over the unknown source location and spectrum.

while assigning larger significance to those events found closest to the time of interest. This two-parameter ranking method frees us from having to choose a fixed search interval. We can also limit the length of the search interval to a value that is computationally reasonable without fear of truncating our probability distribution.

With a false alarm rate of 4.79×10^{-4} Hz for GW150914-GBM, which begins 0.4 s after the time of the GW event, we calculate a false alarm probability for GW150914-GBM, $P = 9.58 \times 10^{-4} \text{ Hz} \times 0.4 \text{ s} \times (1 + \ln(30 \text{ s} / 0.256 \text{ s})) = 0.0022$, where the logarithmic term accounts for the search window trials.

We now explore in detail whether the GBM data for GW150914-GBM suggest an astrophysical origin and whether that source is consistent with GW150914 or can be attributed to other causes.

2.3. Light curve

Figure 3 shows the count rate registered in all 14 GBM detectors, with a zero time centered on the detection time of the GW event GW150914. In Figure 4, the counts are summed over all the detectors. The time binning of 1.024 s was one of three time-scales selected *a priori* during the optimization of the search procedure, and was the most significant time-scale in the detection of GW150914-GBM. We subsequently optimized the phasing of the 1.024 s bins to produce the largest significance, which is higher than the significance in the initial 60 s search window (Figure 2). The shaded region shows this optimized 1.024 s interval.

The three low 1.024 s bins in Figure 4 that precede the high bin are consistent with a normal background fluctuation. Other similar excursions, positive and negative are seen in the panel showing the longer time span. The decrease cannot be caused by anything blocking photons: for the energy range of the figure, only a very bright and hard transient could be strong enough for a single source going behind the Earth to cause a rate decrease. Nor could a data issue have caused the photons to “move” from the low bins to the high bin that we attribute to GW150914-GBM. The GBM hardware time-tags individual photons as they arrive. There is a known GBM hardware anomaly in which dips and peaks in a time history are digitally created. For one second the GBM clock is mis-set by 0.1 s. This has the effect of shifting a block of counts by 0.1 s, leaving a 0.1 s interval with no counts and another 0.1 s interval with double counts – shifted and correct. These “timing glitches” are understood and have been extensively studied since they are readily found by the TGF (Briggs et al. 2013) and GRB offline searches. While there are some variations on this pattern, all timing glitches are definitively revealed by a time interval of duration tens of milliseconds with no counts from any detector. We have examined the data at higher resolution than shown in Figure 4 and no timing glitches are present. We have also investigated any telemetry issues and anomalies suggestive of data problems and we find that everything on the spacecraft and in our ground processing was operating nominally.

The lack of a prominent, bright detector or pair of detectors accounts for the non-detection

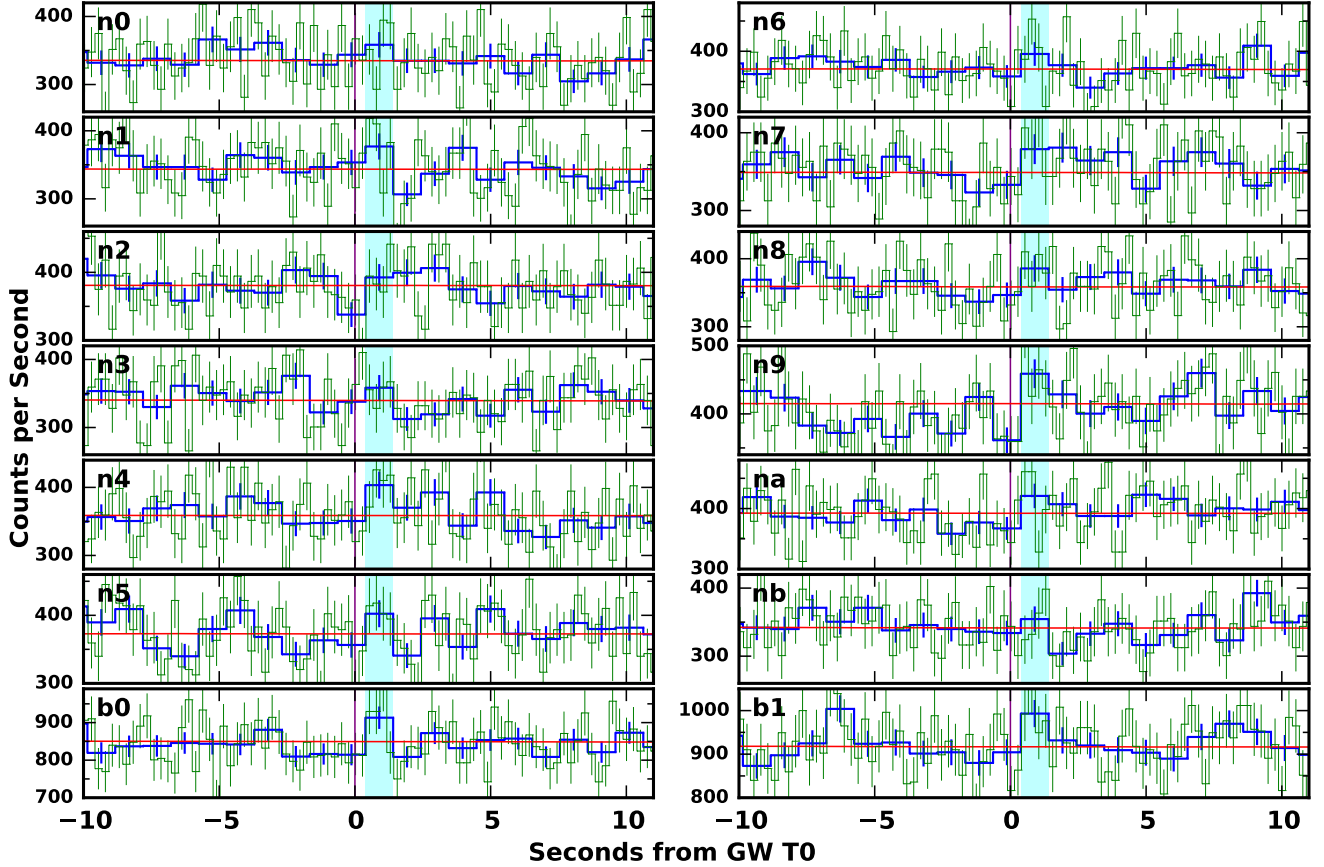


Fig. 3.— Count rates detected as a function of time relative to the detection time of GW150914, in each of the 14 GBM detectors. The shaded region is the time interval of GW150914-GBM, beginning 0.4 s after GW event GW150914. Time bins are 1.024 s wide and the red line indicates the background. The blue lightcurve was constructed from CTTE data, rebinned to optimize the signal-to-noise ratio. The 0.256 s CTIME binning is overplotted on the 1.024 s lightcurve. NaI data are summed over 50 – 980 keV and BGO data over 420 keV – 4.7 MeV. It is noteworthy that all detectors rise above the background level and that no detector stands out. The detector angles to different sky positions on the LIGO localization map are given in Table 2.

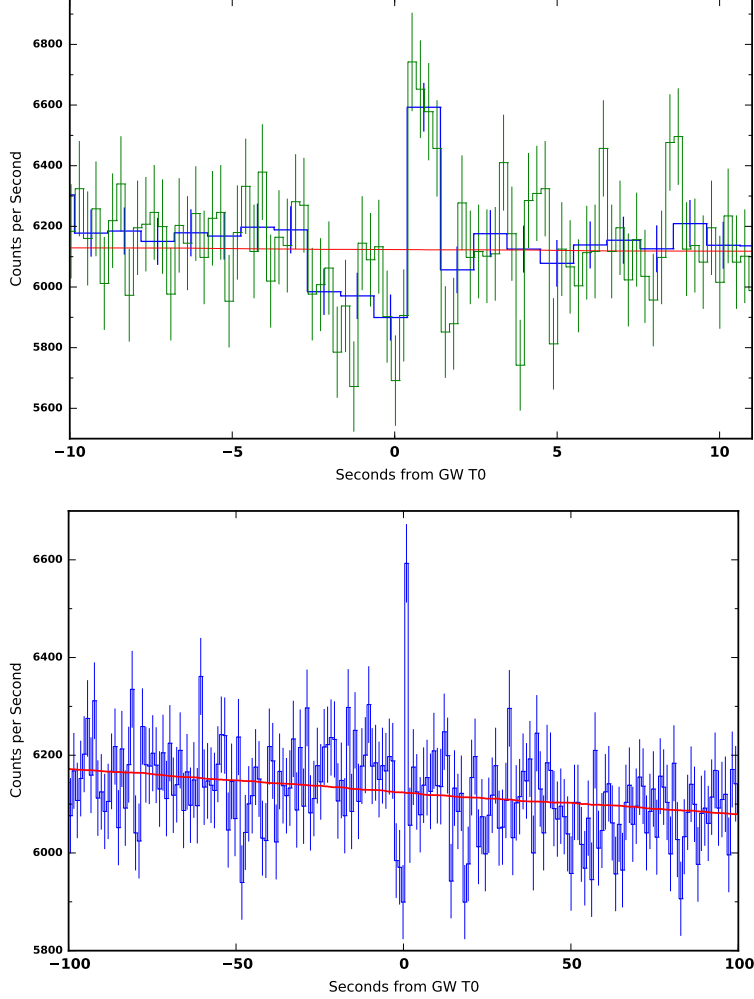


Fig. 4.— Count rates detected as a function of time relative to the detection time of GW150914, summed over all 14 GBM detectors. NaI data are summed over 50 - 980 keV and BGO data over 420 keV – 4.7 MeV. Time bins are 1.024 s wide and the red line indicates the background level. The blue lightcurve was constructed from CTTE data, rebinned to optimize the signal-to-noise ratio. In the top panel, the 0.256 s CTIME binning is overplotted on the 1.024 s lightcurve. The dip before the spike associated with GW150914-GBM is not significant. Such dips are common in stretches of GBM data, as can be seen in the longer stretch of data on the bottom panel. A 1600 s stretch of data centered on GW150914-GBM, with 1.024 s binning, shows 100 runs each of positive and negative dips lasting 3 s or longer relative to a third-order polynomial fit background over the 1600 s time interval, with 55 (38) negative (positive) excursions lasting 4 s or longer.

of this event on-board and in the undirected offline search. None of the detectors reaches the single-detector threshold of the offline search, indicating an event much weaker than the limiting sensitivity of the undirected search. The fact that all the NaI detectors, and both BGO detectors, register counts above the background fit is unusual. We looked through 30 days (1.7 million seconds of livetime) of data for similar features showing high multiplicities of detectors above or below the background level. The signature required both BGOs to exceed background by $\geq 2\sigma$, at least two NaI detectors with $\geq 2\sigma$, and at least six additional NaI detectors with signal levels $\geq 1\sigma$, for a total of eight NaI detectors and two BGO detectors with signal requirements. Three timescales of the 1.024 s binned data: 0.7 s, 1.0 s, and 1.4 s, were searched using four search window phases and five energy ranges, including those in the lightcurve shown in Figure 4.

GW150914-GBM exceeds these requirements (Table 1), with two NaI detectors above 2σ and eight additional NaI detectors above 1σ . The search found 20 candidates (including GW150914-GBM), 14 excesses, and 6 deficits, giving a 90% confidence level upper limit of 27.8 total candidates. If we consider these candidates to be non-astrophysical, this suggests a background rate of one per 6.12×10^4 s implying a chance coincidence of 1.0×10^{-3} for a signal to accidentally match the signature of GW150914-GBM in a 60 s period.

Table 1: Signals in the GBM detectors in σ deviation from a background fit for the 1.024 second interval beginning at 463917049.775000 = 2015-09-14 09:50:45.775000.

NaI 0	NaI 1	NaI 2	NaI 3	NaI 4	NaI 5
1.31	1.81	0.64	1.05	2.42	1.68
NaI 6	NaI 7	NaI 8	NaI 9	NaI 10	NaI 11
1.31	1.64	1.45	2.20	1.61	0.66
BGO 0	BGO 1				
2.25	2.56				

Figures 5 and 6 shows the lightcurve in the summed NaI and BGO detectors, respectively, divided into the eight native CTIME energy channels, with the energy ranges indicated in the panels. These lightcurves show that GW150914-GBM has a very hard spectrum, with little to no signal below 50 keV and a peak in the spectrum for the NaI detectors in the 290 – 540 keV band. Above 300 keV, photons deposit little of their energy in the thin NaI detectors so that the measured energy is much lower than the true incident energy. A significant count rate in this energy band in the NaI detectors implies an incident flux of higher-energy photons, consistent with the BGO count spectrum that extends into the MeV energy range. BGO is a higher-Z material and the detectors are thick, so that incident MeV photons deposit most or all of their energy in the scintillator and the measured energy is a good estimate of the incident energy. Both the NaI and the BGO count spectra look reasonable, with no indications that the event is a statistical fluctuation - there are no gaps in the spectra between 50 keV and 980 keV for the NaI detectors and between 420 keV and 4.7 MeV in the BGO detectors, as one would expect if the event were spurious, and the NaI and BGO energy spectra are consistent with each other.

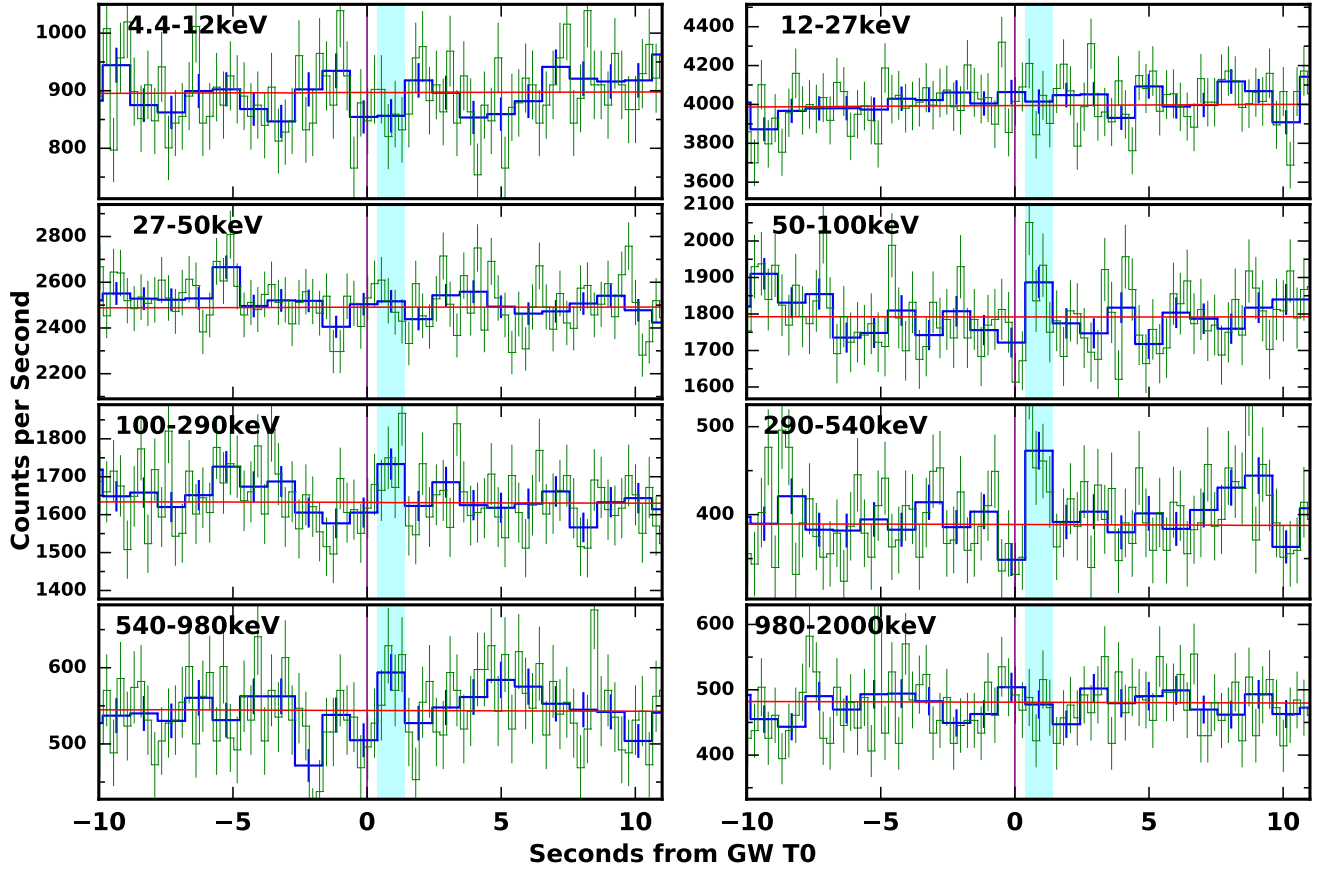


Fig. 5.— Detected count rates summed over NaI detectors in 8 energy channels, as a function of time relative to the start of the GW event GW150914. Shading highlights the interval containing GW150914-GBM. Time bins are 1.024 s in duration, with the 0.256 s CTIME lightcurve overplotted in green, and the red line indicates the background level.

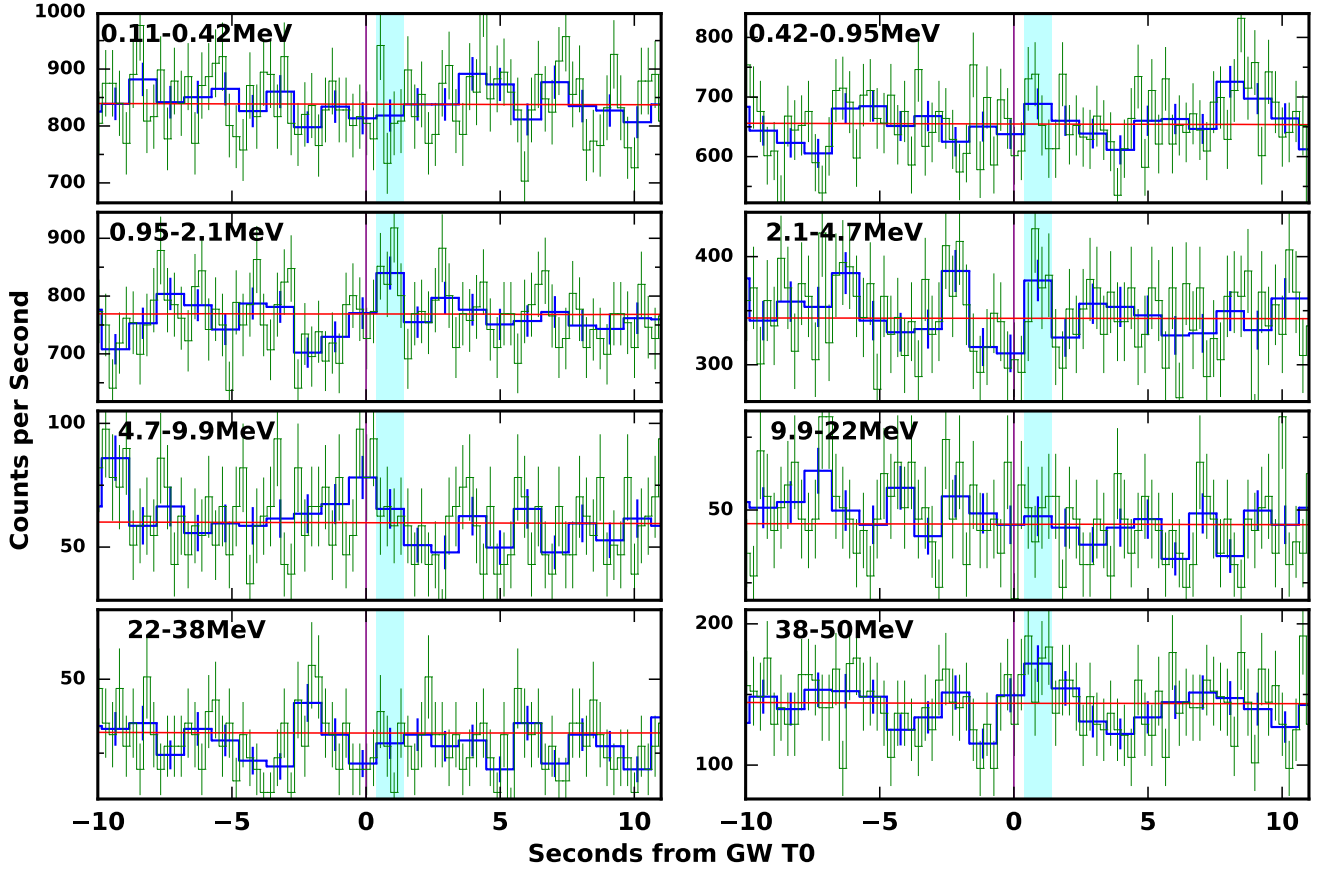


Fig. 6.— Detected count rates summed over BGO detectors in 8 energy channels, as a function of time relative to the start of the GW event GW150914. Shading highlights the interval containing GW150914-GBM. Time bins are 1.024 s in duration, with the 0.256 s CTIME lightcurve overplotted in green, and the red line indicates the background level.

2.4. Localization

The angular response of the NaI detectors allows the reconstruction of the most likely arrival direction of an impulsive event, based on the differences in background-subtracted count rates recorded in 12 NaI detectors that have different sky orientations. The energy range 50 – 300 keV is selected in the standard approach to source localization, both to minimize the effect of short time-scale variability contributed by galactic sources such as Sco X-1, which have steeply falling energy spectra above 20 keV, and to maximize the counts in the energy range where the detector spectral response is very good (response and energy accuracy fall above 300 keV). This energy range captures the peak in the spectral energy distribution for most GRBs. Model rates are calculated for the detector response to sources with the three different energy spectra described in section 2.1. The most likely arrival direction is the one in which χ^2 is minimized in a comparison of background-subtracted observed and model rates on an all-sky grid of 1° resolution, as described in Connaughton et al. (2015). This process yields a localization in both equatorial and galactic coordinates and a 68% statistical uncertainty radius, σ . The uncertainty region covers all the grid points that lie within 2.3 units of the χ^2 minimum, and σ is calculated assuming the uncertainty region is a circle. In practice the uncertainty region can be irregular in shape and, for weak events, it may be composed of disjoint islands, so that σ is a measure of the size of the uncertainty region but is not always a good guide to its shape.

The localization of GW150914-GBM finds a best fit to the hard model spectrum and yields a value of RA, Dec = 57, -22 deg with a 68% statistical uncertainty region over 9000 square degrees ($\sigma = 54^\circ$). In addition to the large uncertainty, the χ^2 suggests a bad fit to the observed rates that would have failed the cut applied in regular GBM data processing. The best-fit location is towards the Earth but the large uncertainty on the location allows an arrival direction from the sky. It can be seen from Figure 3 that the rates in the NaI detectors are not very high above background and the differences among them do not allow much discrimination of arrival direction. GBM detectors register signal counts directly from a source and also record a source signal from gamma rays scattering in the Earth’s atmosphere, with a magnitude determined by the source-Earth-detector geometry. When finding the most likely arrival direction for an event, the localization algorithm fits both a direct and atmospheric component taking into account the position of the Earth in the spacecraft coordinate system at the time of the observation. At the time GW150914-GBM was detected, only one of the NaI detectors had a favorable Earth-viewing angle. The detector normal of NaI 11 was oriented at 39° to the Earth, yet registered the lowest signal above background of any detector, suggesting that whatever the source direction, the atmospheric component was not large. NaI detectors 0 through 5 were not susceptible to any flux from the atmosphere because they faced the sky with the spacecraft positioned between the detectors and the Earth. There is no weighting in the localization algorithm to disfavor the part of the sky that is occulted by the Earth - the algorithm uses only the relative rates in the NaI detectors to reconstruct the most likely arrival direction after modeling the response to both direct and atmospheric components at each tested sky position (even those behind the Earth),

taking into account the position of the Earth when evaluating the atmospheric component.

Since the detection of GW150914, the analysis of the LIGO data has resulted in a refinement of the GW event localization, including a new map (The LIGO Scientific Collaboration and Virgo 2015d) that places most of the probability in the southern portion of the original arc, with only 6% in a northern sliver of the arc. Most of the arc lies at a large angle, θ , to the spacecraft zenith, almost entirely under *Fermi*. Figure 1 shows that part of the southern arc (25% of the probability) is hidden to *Fermi* by the Earth. The rest of the arc lies above the horizon, at low elevation above the Earth to *Fermi*. We note that for sources at low elevation, the atmospheric component of the signal is low relative to the direct component (Pendleton et al. 1999; Harmon et al. 2002), compatible with the low count rate observed in NaI 11. The position RA, Dec = 57, -22 deg returned by the standard process is roughly consistent with the LIGO arc. Different data interval and background selections of the GBM data used in the localization led in some cases to localizations at the spacecraft zenith, an indication that the localization process was not converging.

GBM is a background-limited instrument and this event is much weaker than any GRB we would normally localize based on either an on-board or offline detection. The signal to noise ratio in each detector is low and affected by fluctuations in the background rates. We reported in Blackburn et al. (2015b) that we could not constrain the location of the transient event uncovered in our search. We have, since then, investigated our data more closely.

We do not use the BGO detectors in the standard localization process, because their angular response depends only weakly on the source direction compared to the response of the NaI detectors. Also, because the flux from sources detected by GBM declines with increasing energy and, for GRBs, falls more steeply above $E_{peak} \sim 100 - 500$ keV, source signals are usually more intense in the NaI detectors than in the BGO detectors. For event GW150914-GBM, the signals in individual NaI detectors are weak. The fact that there is a detectable signal in the BGO detectors suggests that if the event is real, then for any reasonable source energy spectrum, it arrived from a direction preferentially viewed by BGO detectors relative to NaI detectors. This picture is compatible with a source direction underneath the spacecraft.

Table 2: Sky locations on LIGO localization arc for GW150914 that are visible to GBM at the time of the GW event. The first 10 are on the southern lobe, which contains 94% of the probability. The positions are 5° apart. Positions are given in equatorial (Right Ascension and Declination) and spacecraft (ϕ , θ) frames. The Large Area Telescope (LAT) boresight is at spacecraft zenith, $\theta = 0^\circ$. Angles to each detector normal are listed for each position, The final column shows the % probability of the LIGO sky map contained in a slice of the arc centered on each position. The final position is on the northern lobe, which contains 6% of the probability of the localization of GW150914. The positions behind the Earth to *Fermi* contain 25 % of the probability and are not listed here. All angles are given in degrees.

RA	Dec	SC ϕ	SC θ	NaI 0	1	2	3	4	5	6	7	8	9	10	11	BGO 0	1	Prob. %
83.98	-72.85	342	160	144.8	122.0	83.1	117.8	76.1	71.2	161.5	142.0	97.3	149.2	103.3	108.6	70.8	109.2	12.1
101.99	-73.87	349	156	139.9	117.1	79.2	115.2	75.4	66.5	161.6	145.5	101.3	149.4	104.1	113.4	66.1	113.9	10.0
118.31	-72.94	354	151	134.9	112.3	75.6	112.0	74.2	61.6	159.9	148.3	105.0	149.3	105.4	118.3	61.3	118.7	10.3
132.04	-70.44	357	147	129.9	107.6	72.4	108.5	72.8	56.7	157.0	150.1	108.3	149.0	106.9	123.2	56.5	123.5	11.2
140.85	-66.63	358	142	125.2	103.3	69.9	104.4	70.7	51.7	153.1	150.5	110.9	148.7	109.0	128.2	51.5	128.5	10.3
147.53	-62.51	359	137	120.3	98.8	67.4	100.3	68.9	46.7	148.8	150.2	113.5	147.5	110.9	133.2	46.5	133.5	7.4
151.18	-57.97	358	132	115.5	94.5	65.5	96.0	66.9	41.7	144.3	148.8	115.6	146.2	113.0	138.2	41.5	138.5	5.8
153.363	-53.091	360	127	111.2	90.8	64.7	91.2	64.0	37.0	139.4	145.9	116.5	145.2	115.9	142.9	36.7	143.3	3.7
153.933	-48.239	359	122	106.7	87.1	64.0	86.6	61.6	32.2	134.5	142.8	117.4	143.5	118.4	147.7	31.8	148.2	1.8
155.331	-43.208	358	116	102.5	83.7	64.1	81.7	58.6	27.7	129.5	138.9	117.4	141.9	121.4	152.1	27.1	152.9	2.0
151.172	-7.256	342	84	75.4	66.7	76.2	45.6	39.5	21.9	93.6	105.2	105.6	124.1	141.1	157.9	18.7	161.3	4.8

We performed simulations to quantify how well we expect to localize weak signals that come from directions along the LIGO arc. We divide the LIGO arc into 11 positions, 10 on the southern portion, one in the north, excluding the parts of the arc that were occulted to *Fermi*. The positions are listed in Table 2, which shows each position in celestial equatorial and spacecraft coordinates, the angle to each of the NaI and BGO detectors, and the probability of the LIGO source location lying near each position, based on the LIGO location map. The positions are $\sim 5^\circ$ apart, comparable to the accuracy with which GBM could localize a weak triggered transient source using the standard localization techniques. It can be seen that NaI 5 is the only NaI detector with a source angle less than 60° for several of the southern lobe positions. Above an incidence angle of 60° , the angular response of the NaI detectors drops significantly. The detectors are, however, not shielded and thus register counts from any angle, including through the back of the detectors, which can detect gamma rays or cosmic rays with about 20% efficiency relative to on-axis particles.

We calculate the expected count rates in each detector between 50 and 300 keV using the detector responses for each of the 10 positions along the southern lobe of the LIGO arc using a normalization based on the observed event signal. For each position, we add background rates derived from the observed background rate at the time of the detection of GW150914-GBM, and apply Poisson fluctuations to both source and background in 1000 iterations of the 1 s event at each position. Using the background-subtracted count rates in each simulated event, we assess how well we are able to localize such a weak source using our standard localization process. The majority of the simulated events are reconstructed near the arc containing the true positions, with large uncertainties. Count rate fluctuations can lead to poor localizations in the wrong part of the sky. We note that a significant number of simulated events (17%) are placed behind the Earth. A simulation of the final position in Table 2 covering the northern lobe of the LIGO arc places 4% of the localizations behind the Earth but, unlike the southern lobe, these localizations behind the Earth have consistently large σ and bad χ^2 . We conclude that the localization of the observed event GW150914-GBM behind the Earth with a large uncertainty region of 9000 square degrees is not inconsistent with an origin along the LIGO localization arc, most likely on the southern lobe.

GBM was not designed to detect sources under the spacecraft, at large angular offset, θ , to the spacecraft zenith. The pre-launch plan for *Fermi* nominal operations was to observe at a 30° angle from the local zenith, allowing the sky to drift across the field-of-view, rocking the spacecraft north and south on alternate 90 minute spacecraft orbits to achieve even sky coverage for the Large Area Telescope (LAT) survey of the high-energy sky. The GBM detectors were placed for maximum sensitivity to sources in the LAT field-of-view ($\theta = 0 - \sim 65^\circ$), with good sensitivity out to $\theta < \sim 120^\circ$. The Earth was expected to block the high θ regions, which are, by design, not well-viewed by the NaI detectors. The sky survey mode was changed after launch to alleviate the effect of higher-than-expected battery temperatures on the mission lifetime. A 50° rocking profile was found to keep the batteries cooler and is now the nominal sky survey mode, with the result that GBM has more exposure to sky regions at high θ angles than expected when

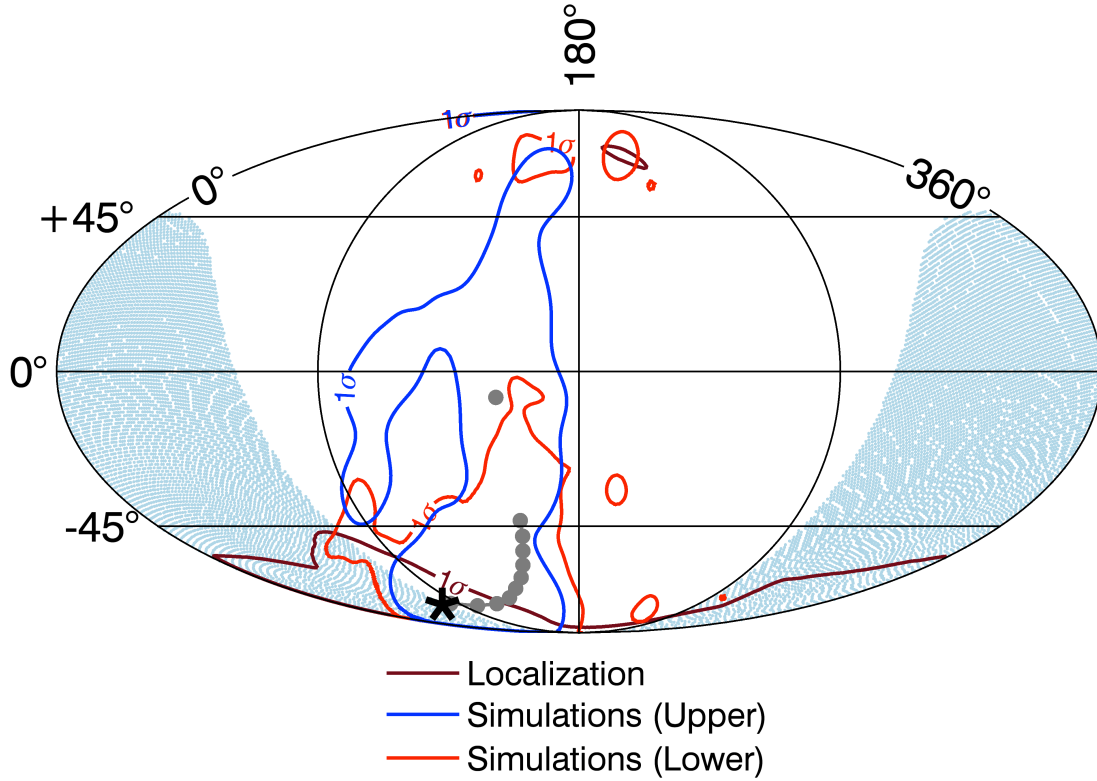


Fig. 7.— GBM localization of GW150914-GBM using NaI detector counts in the 100 – 1000 keV energy range, shown in celestial coordinates. The most favored sky location is marked with an asterisk and the black contour indicates the 68% confidence level region for this localization. The best GBM localization is just behind the Earth’s limb with a large uncertainty contour that significantly overlaps the southern lobe of the LIGO location arc (indicated as 11 grey circles). Simulations of the localization of a weak source from each of these 11 positions along the LIGO localization arc indicate how well GBM localization is expected to perform for a source as weak as GW150914-GBM with the same source geometry relative to the spacecraft. The red and blue contours show the 68% containment for the simulated locations from the southern (lower) and northern (upper) lobe, respectively. The GBM localization overlaps both sets of simulated localizations, with a better match to those from the southern lobe.

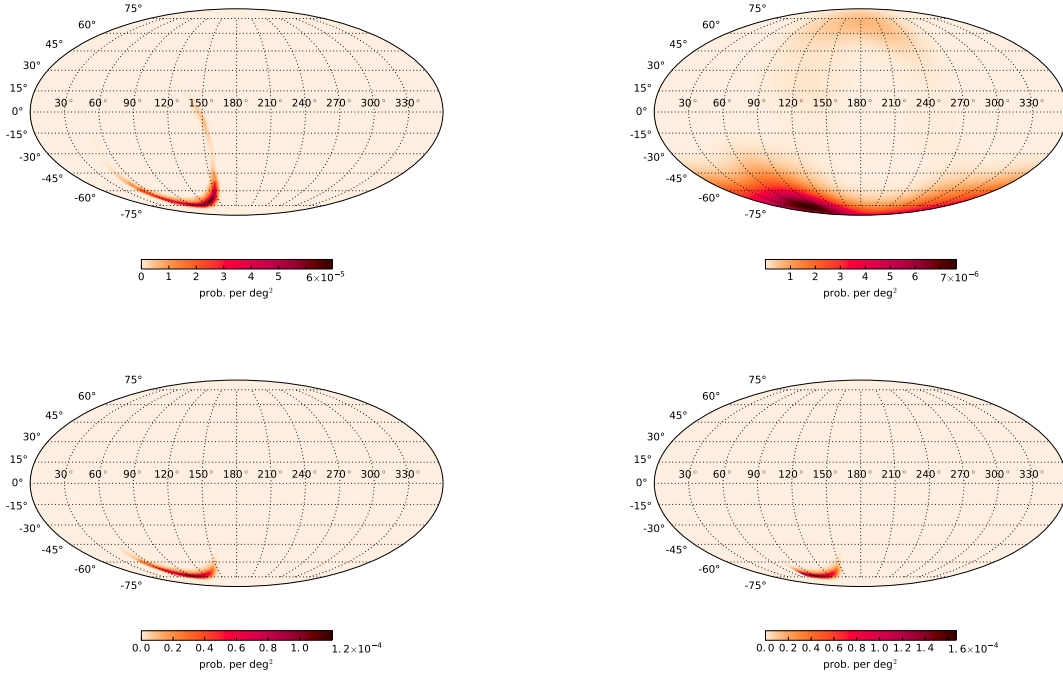


Fig. 8.— The LIGO localization map (top left) can be combined with the GBM localization map for GW150914-GBM (top right) assuming GW150914-GBM is associated with GW event GW150914. The combined map is shown (bottom left) with the sky region that is occulted to *Fermi* removed in the bottom right plot. The constraint from *Fermi* shrinks the 90% confidence region for the LIGO localization from 601 to 199 square degrees.

deciding the detector placement. The combination of the declining sensitivity of the NaI detectors at large angles to the detector normals and the two-detector on-board trigger requirement results in very few GRBs being detected with arrival directions at very high θ . Of the 1776 GRBs listed in the Browse Table at the HEASARC⁸, only 67 occur at a larger θ than 130° , and only 3 larger than 160° .

We attempt to refine the GBM localization by examining a broader energy range than the standard 50 – 300 keV. Noting from Figure 5 that much of the observed signal occurs above 300 keV, we produced model rates using the soft, medium, and hard spectral models in various energy bands, between 50 – 1000 keV, 50 – 540 keV, 100 – 1000 keV, and 100 – 540 keV. We used the standard localization procedure, minimizing χ^2 for the observed rates in each of the energy ranges relative to the model rates in that energy range. The localization in each case returns a similar position for the most likely origin of the source, always slightly behind the Earth, and always at $\theta \sim 160^\circ$. The probability contours are more bounded than those from the 50 – 300 keV localization. The probability maps cover similar regions of sky for all four localizations. The smallest statistical uncertainty was found using the 100 – 1000 keV energy band. A minimum was found at RA, Dec = 75, -73 deg with a 68% confidence region covering about 3000 square degrees ($\sigma = 30^\circ$) and a preference for the hard spectral model. The uncertainty contours are broad but constraining. With a source this weak from this direction in the spacecraft frame, we reach the limit of being able to use the angular response of the NaI detectors to localize a source. The measurement of equal rates in most NaI detectors allows the localization to converge to a region under the spacecraft with slight discrimination in favor of one or another detector cluster but no further refinement. We can, however, say that the general source direction is consistent with the LIGO arc and define a fairly large region on the sky from which the signal must originate.

We include only statistical uncertainties in our location map. The standard localization process using the 50 – 300 keV energy range was found to have a systematic component on the order of 3 – 4° for a sample of 200 triggered GRBs (Connaughton et al. 2015). We do not expect the systematic error to be much different using the 100 – 1000 keV energy range, particularly when compared to the size of the statistical uncertainty when localizing an event this weak, but we note that our characterization of triggered GRB localizations may not be applicable to these weak events that are more affected by background fluctuations comparable in size to the signal strength. Additionally, although the localization uses the standard GBM procedure, the quality of the localizations has not been assessed using non-standard energy ranges and our uncertainty calculations do not include any systematic component.

Figure 7 shows the best position and the associated 1σ uncertainty contours for the localization performed using data between 100 and 1000 keV. The parts of the LIGO arc visible to *Fermi* are shown as a series of points (with positions listed in Table 2) and the Earth region is shaded. The LIGO arc overlaps the GBM localization in the southern lobe. We also show the 68%

⁸<http://heasarc.gsfc.nasa.gov/W3Browse/fermi/fermigtrig.html>

containment region of all the localizations returned by our simulations of weak sources from positions on the southern and northern lobes. The simulations suggest a broad distribution of possible locations for a given source position, but we find that the actual localization of GW150914-GBM is quite well constrained to the part of the sky (and Earth) at high θ , consistent with an origin in the southern lobe. If we assume that GW150914-GBM and GW150914 are related, the two location probability maps can be combined to reduce the 90% confidence level LIGO map area by 2/3, from 601 square degrees to 199 square degrees, as shown in Figure 8.

2.5. Energy spectrum of GW150914-GBM

The data for GW150914-GBM imply a weak but significant hard X-ray source with a spectrum that extends into the MeV range and a location that is consistent with an arrival direction along the southern lobe of the sky map for the GW event GW150914. Converting the observed counts in the GBM detectors to a source flux requires a deconvolution of the instrumental response with an assumed spectral model. We sample a range of arrival directions along the observed LIGO location arc, using the data and associated responses for the detectors at each location that are most favorably oriented to the arrival direction. Table 2 suggests that NaI 5 and BGO 0 are a suitable detector set for all the locations along the arc. We use the `rmfit` spectral fitting package⁹, which takes a forward folding approach to determine the parameters that best fit the data for any model, given the instrumental response. The minimization routine producing the best fit parameters uses a likelihood-based fitting statistic, `CSTAT`.

Because the event is very weak, we do not attempt to fit the full-resolution data (128 energy channels). Instead, we bin the CTTE data into the eight native CTIME energy bins. and use the CTIME energy responses in our fits. GRB spectra are well represented by empirical functions with power-law components around a peak energy in the spectral energy distribution, E_{peak} . The Band function is used when there are enough counts to constrain all parameters, particularly the high-energy power-law index, β . If β is not constrained, a power-law fit with an exponential cut-off above E_{peak} , called the Comptonized model, generally works well. For the weakest bursts, or when E_{peak} lies outside the energy range of the instrument, a power-law fit is adequate and serves to provide an estimate of the flux and fluence of the burst as long as the energy range over which the flux and fluence are calculated is not extended outside the observation range. We find that for all 11 positions along the LIGO arc, a power-law fit to the data from GW150914-GBM can be constrained. For one of the positions, we can also provide weak constraints for a fit to the Comptonized model. Figure 9 shows a representative count spectrum and power-law model fit, with a deconvolution assuming the source lies near the central position of the southern arc. For each of the 11 positions along the arc, we find the best-fit power-law index and associated amplitude. We use these parameters to simulate each spectrum 10^4 times, using the resulting

⁹<http://fermi.gsfc.nasa.gov/ssc/data/analysis/rmfit/>

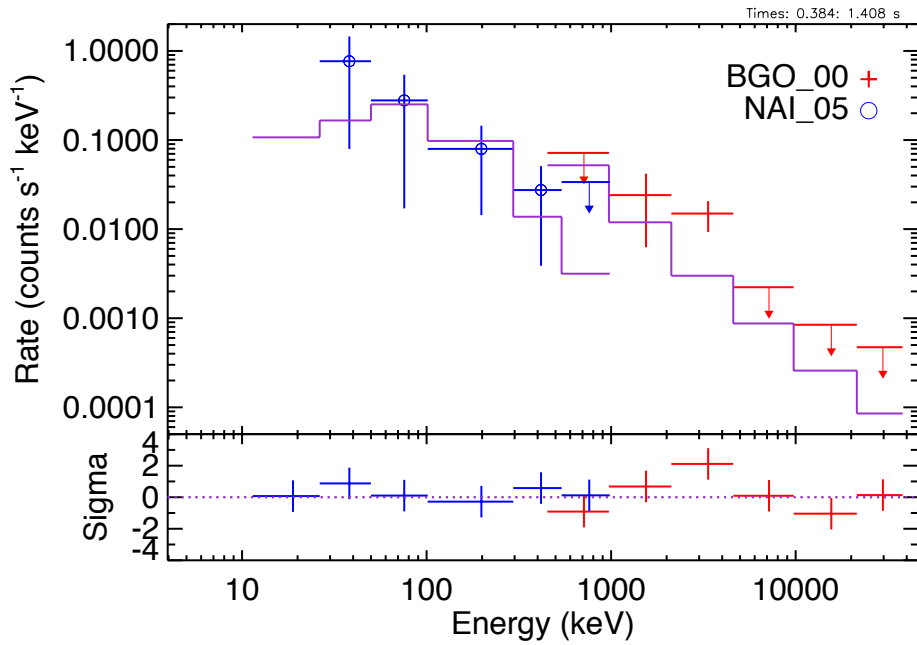


Fig. 9.— Power-law fit to the data from NaI 5 (blue) and BGO 0 (red) for the time interval $T_0+0.384$ to $T_0+1.408$. The symbols show the data. The solid line shows the best-fit power-law model. Residuals on the bottom panel show scatter but no systematic deviation. We cannot use the top and bottom energy channels in either detector data type (there are threshold effects and electronic overflow events), leaving the data from 12 energy channels included in the fit.

distribution to estimate the uncertainties on the parameter values. We also sample the parameter distributions to calculate the fluence and its confidence region, weighting the sampling along the arc according to the LIGO localization probability contained near each point on the arc. We obtain a best-fit power-law index $-1.40^{+0.18}_{-0.24}$ and amplitude $0.002^{+0.002}_{-0.001}$ photons $\text{s}^{-1} \text{cm}^{-2} \text{keV}^{-1}$ over the LIGO localization arc, yielding a fluence between 10 and 1000 keV of $2.4^{+1.7}_{-1.0} \times 10^{-7} \text{erg cm}^{-2}$.

For a deconvolution assuming a source position at the northeastern tip of the southern lobe (entry 10 in Table 2), the Comptonized model converges to find a best fit E_{peak} of $3.5^{+2.3}_{-1.1}$ MeV with a power-law index below E_{peak} of $-0.16^{+0.57}_{-0.50}$. The fluence obtained assuming a Comptonized model for a source from this position is $2.8^{+1.0}_{-0.9} \times 10^{-7} \text{erg cm}^{-2}$.

The fit parameter values are typical for short GRBs, with power law indices of about -1.4 found in cases where the GRB is too weak to constrain E_{peak} , and values for the Comptonized fit parameters that are also typical of short GRBs (Gruber et al. 2014). A fluence of $2.4 \times 10^{-7} \text{erg cm}^{-2}$ is nearly average for short GRBs, with 40% of short GRBs detected by GBM weaker than this value¹⁰. The least energetic short GRBs detected by GBM have a fluence an order of magnitude smaller than GW150914-GBM. If GW150914-GBM is part of the short GRB population, then its fluence is not atypical but its unfortunate arrival direction yields only a weak signal in GBM. Figure 9 shows the model is a reasonable fit to the count spectrum even at low energies, implying no paucity of counts at low energies in NaI 5, which is the only detector with a small enough viewing angle to the source position to have any sensitivity below 50 keV.

At a distance of 410^{+160}_{-180} Mpc implied by the GW observations (Abbott et al. 2016), we obtain a source luminosity between 1 keV and 10 MeV of $1.8^{+1.5}_{-1.0} \times 10^{49} \text{erg s}^{-1}$. The uncertainties reflect the range of possible distances to the progenitor, uncertainties in the spectral fit parameters and the range of arrival directions along the arc.

2.6. Other observations of GW150914-GBM

Instruments other than GBM can also detect impulsive events in the hard X-ray energy range. No pointed instruments reported detections of GW150914, suggesting they were not looking in that direction at the time of the GW event. The anti-coincidence shield (ACS) on the INTEGRAL spacecraft has a large collection area above 80 keV with an all-sky response that is not hindered by Earth occultation. We looked for a signal in INTEGRAL-ACS at the time of GW150914-GBM and found no excess above background¹¹. The INTEGRAL-ACS team reported a fluence limit of $1.3 \times 10^{-7} \text{erg cm}^{-2}$ in the 100 keV – 100 MeV energy range based on a null detection over a 1 s period (Ferrigno et al. 2015). This is lower than the value

¹⁰<http://heasarc.gsfc.nasa.gov/W3Browse/fermi/fermigbrst.html>

¹¹<http://isdc.unige.ch/~savchenk/spiacs-online/spiacs-ipnlc.pl>

$3.8_{-2.3}^{+2.9} \times 10^{-6}$ erg cm⁻² obtained by propagating the fluence of GW150914-GBM into the 100 keV – 100 MeV range using the power-law function fit to the GBM data. Because power-law fits without a break are generally not physical representations of a source spectrum, a fluence calculation extending the power-law fit outside the observed energy range may not be realistic. Instead, we fit a Band function to the GBM data, fixing the parameter values to those used by the INTEGRAL team for their upper limit calculation in Ferrigno et al. (2015), $(\alpha, \beta, E_{peak}) = (-1, -2.5, 500 \text{ keV})$, and fitting only the amplitude. We find a fluence between 10 and 1000 keV ranging from $1.4 \pm 0.6 \times 10^{-7}$ erg cm⁻² to $4.4 \pm 1.8 \times 10^{-7}$ erg cm⁻² depending on the source position on the LIGO arc. This translates to a fluence between 100 keV and 100 MeV ranging from $2.0 \pm 0.8 \times 10^{-7}$ erg cm⁻² to $6.2 \pm 2.5 \times 10^{-7}$ erg cm⁻², consistent with the INTEGRAL upper limit at all but the southwestern parts of the LIGO location arc.

Additionally, a search of the INTEGRAL-ACS data revealed a detection rate of only 55% of GBM-detected weak short GRBs (Briggs et al., in preparation). We do not consider, therefore, the non-detection of GW150914-GBM by INTEGRAL-ACS, a sufficient reason to reject our candidate.

2.7. Possible origins for GW150914-GBM

The energy spectrum of GW150914-GBM is too hard for any of the galactic transient sources detected by GBM, either bursts from magnetars, type I thermonuclear X-ray bursts, or outbursts from accreting pulsars, and also too hard to be of solar origin. Additionally, the sun was quiet around the time of the GW event detection. The localization (section 2.4) close to the Earth’s limb raises the question of whether GW150914-GBM comes from the Earth.

Terrestrial Gamma-ray Flashes emit gamma rays extending to at least 40 MeV. TGFs are detected either as gamma rays produced by electrons accelerated in electric fields in thunderstorms, or as secondary electrons and positrons guided by the magnetic field line that connects a thunderstorm to a gamma-ray detector. Typical durations for the gamma-ray and electron events are several hundred μs and several to tens of ms, respectively, much shorter than GW150914-GBM (Briggs et al. 2013). TGF gamma rays are detected by GBM when the source is within 800 km of the Fermi nadir; the charged particle form can be detected from thousands of kilometers from the source, but only when GBM is within the ~ 100 km diameter beam centered on the magnetic field line from the source (Dwyer et al. 2008; Briggs et al. 2011; Briggs et al. 2013). The World Wide Lightning Network (WWLLN; Rodger et al. (2009); Hutchins et al. (2012)), a global network of VLF radio receivers, virtually always finds clusters of lightning (i.e., thunderstorms) for GBM TGFs. At the time of GW150914-GBM WWLLN has no lightning detections over ± 10 minutes within 800 km of the spacecraft nadir nor at the two magnetic footprints, making it very unlikely that there were TGF sources within GBM’s detection range.

Another lightning detection network, GLD360 (Said et al. 2010, 2013), reported a very high peak

current lightning stroke at 09:50:45.406 at latitude 11.1685, longitude -3.2855 degrees. At more than 4000 km from *Fermi*, this is past the horizon so that gamma rays would be blocked by the Earth. The magnetic field line from this source is thousands of kilometers to the west of *Fermi*, so if any charged particles were emitted, they would not be transported to *Fermi*.

At the time of the GW event *Fermi* was at low geomagnetic latitude and was not near the SAA. While we cannot exclude a magnetospheric origin for GW150914-GBM, the observing conditions were not conducive to such an event, nor is the lightcurve typical of magnetospheric activity, which is usually manifested as longer and smoother (10s of seconds) bumps above background.

2.8. Search for steady emission from known or unknown sources near the LIGO localization region

Using various search techniques, we found (i) no evidence for long-term steady emission from the direction of GW150914-GBM, (ii) no evidence for contamination by known sources of hard X-ray emission of any search for emission related to GW150914-GBM, and (iii) no evidence for non-impulsive emission related to the GW event event in the days surrounding the event.

In addition to GBM’s role as a powerful detector of transient, impulsive sources, the Earth Occultation technique (EOT) allows GBM to perform as an all-sky monitor of sources emitting hard X rays at levels typically undetectable above the GBM background. This technique involves modeling the GBM background count rates when a potential source of hard X rays sets or rises from behind the Earth. Candidate sources are monitored¹² with around 100 significantly detected to date above 10 mCrab between 12 and 25 keV (Wilson-Hodge et al. 2012). Of the 246 sources that are monitored, six lie within 5° of the LIGO localization region for GW150914: LMC X-2, RX J0520.5-6932 (which was detected in hard X-ray emission by *Swift* Burst Alert Telescope (BAT) in 2013¹³), the flat spectrum radio quasar PKS 0601-70, the gamma-ray binary system 2FGL J 1019.0-5856, and the accreting X-ray binary pulsars GRO J1008-57 and RX J0520.5-6932. Only GRO J1008-57 has previously been detected by GBM through the EOT. Both of the accreting pulsars lie within 3° of the LIGO error region and have been detected in the past through the GBM pulsar monitoring program, which is more sensitive to pulsed emission than the EOT is to non-pulsed emission. We looked for pulsed emission from these accreting pulsars on 2015 September 14 and find they are not currently active. We also used a blind frequency search for pulsed emission from 24 positions along the Galactic plane and from the direction of the Small and Large Magellanic clouds. We did not detect any signal within or near the LIGO localization region. In any search for long-lived emission in the days around the detection of the GW event, we do not, therefore, expect contamination from known sources of

¹²<http://heastro.phys.lsu.edu/gbm/>

¹³<http://swift.gsfc.nasa.gov/results/transients/>

hard X-ray emission above the GBM EOT and accreting pulsar detection thresholds.

The daily sensitivity of the EOT is about 100 mCrab. The EOT can resolve signals from sources 2° apart. We divided the full LIGO arc into 34 resolvable positions (all but one along the southern lobe of the arc) and looked for mission-long activity from these positions, as well as daily emission around the time of the GW event. We examined 3 years of data using the EOT, from 2013 January 1 through 2016 January 29. Long-term averages were consistent with no detections for the 12 – 25, 25 – 50, 50 – 100, 100 – 300, and 300 – 500 keV energy bands. We also looked for emission on a daily time-scale for the month of September 2015 without detecting any of the sources during the month surrounding the LIGO GW event time.

The Earth occultation technique fails to measure source fluxes if the angle between the tangent to the Earth’s limb and the spacecraft orbit normal, β , exceeds 66.5° . At grazing incidence, the Earth occultation transition becomes too extended in time (>20 s from 100% – 0% atmospheric transmission), and at β values beyond grazing incidence, the source is not occulted by the Earth at all. This occurs at certain points in the 50-day *Fermi* orbital precession cycle for high declination sources ($> \pm 40^\circ$) owing to the relative geometry of the source position and the Fermi orbital inclination of 26.5° . Only 13 of the targets, with right ascensions from $48 - 77^\circ$, and the northern lobe position, had usable Earth occultation measurements spanning the time of the LIGO event. The remaining targets with right ascensions from $74 - 155^\circ$ had no usable Earth occultation measurements from before the time of the LIGO event until 2 or more days after GW150914. Another way to look at this is that these unocculted positions never set behind the Earth and were observed by GBM with 85% exposure, losing only the time that *Fermi* crossed through the SAA. For much of the LIGO arc during the days around the GW event detection, GBM was thus exceptionally sensitive to any impulsive emission that would have triggered the instrument.

If GW150914-GBM is related to the GW event, and the localization is in the region of the LIGO arc with $\beta \sim 66.5^\circ$, then grazing Earth occultations could be responsible for the non-detection of flux below 50 keV (Figure 3). Lower energy photons, e.g. 12 – 25 keV can be fully blocked (0% atmospheric transmission) before the 100 – 300 keV band reaches 50% transmission. We cannot exclude the possibility that the spectral analysis (and thus the luminosity estimate) is affected by partial, energy-dependent atmospheric absorption of the signal, but the spectral deconvolution of the data from NaI 5 (section 2.5) does not suggest a deficit of counts below 50 keV relative to the model, so it is more likely that the hard spectrum observed in most of the detectors is a mixture of intrinsic spectral hardness and the large viewing angles to most of NaI detectors that lead to preferential detection of higher-energy photons and absorption of photons of lower energy before they reach the scintillator.

The LIGO localization arc for GW event GW150914 became observable by the *Fermi* LAT ~ 4000 s after the GW event and a search for high-energy emission over time-scales comparable to our search in hard X rays with the EOT is reported by The *Fermi*-LAT Collaboration (2016).

3. Discussion and outlook for joint LIGO-GBM science

GBM observed over 75% of the probability in the GW event sky location at the time of GW150914. A weak hard X-ray source lasting around 1 s was detected above 50 keV 0.4 s after the GW event using a technique developed to find short transients in the GBM data in coincidence with sub-threshold GW events. The GBM signal is localized to a region consistent with the LIGO sky map, with a large uncertainty on the location. If the transient event uncovered in the GBM data is associated with GW150914, then it is possible its origin under the *Fermi* spacecraft, combined with the weakness of the source, can account for the lack of confidence associated with the standard localization procedure applied to this event. If we assume the LIGO and GBM events have a common origin, then combining the LIGO and GBM localization maps reduces the LIGO localization area by 2/3.

The transient event cannot be attributed to other known astrophysical, solar, terrestrial, or magnetospheric activity. The distribution of detected counts as a function of energy appears reasonable among detectors across the energy range 50 keV – 4.8 MeV. Spectral deconvolution yields a fluence over the 1 s duration of $2.4_{-1.0}^{+1.7} \times 10^{-7}$ erg cm⁻², comparable to moderate intensity short GRBs on which GBM has triggered. This implies that with a more favorable arrival geometry, this event could have triggered GBM on-board at the time of the GW detection, providing a real-time localization within seconds of the trigger. The real-time location could assist follow-up observers, reducing the number of observations needed to cover the LIGO localization region.

The detection of an electromagnetic counterpart to a merger of stellar mass black holes would be a surprising event. Although circumbinary disks are expected to form around supermassive black holes (Mayer et al. 2007), there is no such prediction for stellar mass systems. Moreover, the GBM signal appears similar to a short GRB, in duration (less than 2 s), and in energy spectrum (peaked near an MeV). Models for short GRBs from compact binary progenitors always involve a neutron star, with short GRBs more easily produced from two neutron stars, unless the black hole companion has a high initial spin (Giacomazzo et al. 2013). A luminosity of $1.8_{-1.0}^{+1.5} \times 10^{49}$ erg s⁻¹ for a short GRB, assuming the source distance of 410_{-180}^{+160} Mpc implied by the GW observations (Abbott et al. 2016), is an order of magnitude dimmer than the peak luminosities of the dimmest short GRBs in the sample analyzed by Wanderman and Piran (2015).

Further observations by LIGO and Virgo in coincidence with a detector sensitive to hard X-ray or gamma-ray transient events will determine whether short bursts of high-energy electromagnetic radiation accompany stellar mass black hole binary mergers. Because of the weakness of GW150914-GBM and its large localization uncertainty, chance coincidence may play a role in both the identification of GW150914-GBM as an astrophysical phenomenon and its association with the GW event, even with the false alarm probability of 0.0022 that we calculate in section 2.2. If the association is real, then the alignment of the merger axis with our line of sight is serendipitous. Another possibility is that the electromagnetic emission is not narrowly collimated

and we can expect further joint detections of stellar mass black hole binary mergers and GRBs. This paradigm may be in tension with the non-detection of GW candidates in the last science runs of the previous configuration of LIGO/Virgo, S6/VSR2&3 (Abadie et al. 2012). None of the GRBs with known redshift detected during S6/VSR2&3 was within the BBH detection horizon (100 Mpc). It is possible, however, that some of the 90% of GRBs with unknown redshifts were within this horizon.

Analysis of the GBM data corresponding to all sub-threshold GW events from the O1 initial science operation period of LIGO is in progress. We have developed pipelines and data products to rapidly search the GBM data for counterparts to any GW events and communicate their localization to electromagnetic observers within hours of the GW event (depending on data downlink from the *Fermi* spacecraft).

Given the detection of GW150914 as a GW event from a stellar mass black hole binary system, then with all but the most pessimistic predictions, the detection of the weaker GW signals from neutron star binary systems is expected no later than 2019, when LIGO/Virgo reach full sensitivity. If this detection occurs during O2, the second observing run of LIGO and the initial deployment of Virgo, expected later in 2016, our GBM-LIGO/Virgo pipelines are ready. Even if the association between GW150914-GBM and GW150914 is spurious, we expect to detect short GRBs from neutron star binary systems. With its broad field-of-view and good sensitivity at the peak emission energies for short GRBs, *Fermi* GBM is an ideal partner in the search for electromagnetic signals in coincidence with gravitational wave detections. Joint observations by *Fermi* and LIGO/Virgo will either confirm or exclude the connection between compact binary systems and short GRBs within a few years.

The GBM project is supported by NASA. Support for the German contribution to GBM was provided by the Bundesministerium für Bildung und Forschung (BMBF) via the Deutsches Zentrum für Luft und Raumfahrt (DLR) under contract number 50 QV 0301. A.v.K. was supported by the Bundesministeriums für Wirtschaft und Technologie (BMWi) through DLR grant 50 OG 1101. HFY acknowledges support by the DFG cluster of excellence “Origin and Structure of the Universe”. AG is funded through the NASA Postdoctoral Fellowship Program.

The authors wish to thank the World Wide Lightning Location Network (<http://wwlln.net>), a collaboration among over 50 universities and institutions, for providing the lightning location data used in this paper. The authors wish to thank L. Blackburn for critical contributions to the analysis and extensive help with the paper.

REFERENCES

- J. Abadie, B. P. Abbott, R. Abbott, T. D. Abbott, M. Abernathy, T. Accadia, F. Acernese, C. Adams, R. X. Adhikari, C. Affeldt, and et al. Search for Gravitational Waves

- Associated with Gamma-Ray Bursts during LIGO Science Run 6 and Virgo Science Runs 2 and 3. *ApJ*, 760:12, November 2012. doi: 10.1088/0004-637X/760/1/12.
- B. P. Abbott, R. Abbott, T. D. Abbott, M. R. Abernathy, F. Acernese, K. Ackley, and C. Adams. Observation of Gravitational Waves from a Binary Black Hole Merger. *Phys. Rev. Lett.*, 116:061102, Feb 2016. doi: 10.1103/PhysRevLett.116.061102. URL <http://link.aps.org/doi/10.1103/PhysRevLett.116.061102>.
- F. Acernese, M. Agathos, K. Agatsuma, D. Aisa, N. Allemandou, A. Allocca, J. Amarni, P. Astone, G. Balestri, G. Ballardin, and et al. Advanced Virgo: a second-generation interferometric gravitational wave detector. *Classical and Quantum Gravity*, 32(2):024001, January 2015. doi: 10.1088/0264-9381/32/2/024001.
- D. Band, J. Matteson, L. Ford, B. Schaefer, D. Palmer, B. Teegarden, T. Cline, M. Briggs, W. Paciesas, G. Pendleton, G. Fishman, C. Kouveliotou, C. Meegan, R. Wilson, and P. Lestrade. BATSE observations of gamma-ray burst spectra. I - Spectral diversity. *ApJ*, 413:281–292, August 1993. doi: 10.1086/172995.
- E. Berger, W. Fong, and R. Chornock. An r-process Kilonova Associated with the Short-hard GRB 130603B. *ApJ*, 774:L23, September 2013. doi: 10.1088/2041-8205/774/2/L23.
- L. Blackburn. Significance of two-parameter coincidence. <https://dcc.ligo.org/LIGO-T1500534/public>, 2015.
- L. Blackburn, M. S. Briggs, J. Camp, N. Christensen, V. Connaughton, P. Jenke, R. A. Remillard, and J. Veitch. High-Energy Electromagnetic Offline Follow-Up of Ligo-Virgo Gravitational-Wave Binary Coalescence Candidate Events. *ApJS*, 217:8, March 2015a. doi: 10.1088/0067-0049/217/1/8.
- L. Blackburn, Briggs M. S., Burns E., Camp J., Christensen N., Connaughton V., Goldstein A., Littenberg T., Veitch J., Racusin J., Shawhan P., Singer L., and Zhang B.-B. LIGO/Virgo G184098: Fermi-GBM ground-based follow-up. *GRB Coordinates Network*, 18339, 2015b.
- M. S. Briggs, V. Connaughton, C. Wilson-Hodge, R. D. Preece, G. J. Fishman, R. Marc Kippen, P. N. Bhat, W. S. Paciesas, V. L. Chaplin, C. A. Meegan, A. von Kienlin, J. Greiner, J. R. Dwyer, and D. M. Smith. Electron-positron beams from terrestrial lightning observed with Fermi GBM. *Geophys. Res. Lett.*, 38:L02808, 2011. doi: 10.1029/2010GL046259. URL <http://onlinelibrary.wiley.com/doi/10.1029/2010GL046259/abstract>.
- M. S. Briggs, S. Xiong, V. Connaughton, D. Tierney, G. Fitzpatrick, S. Foley, J. E. Grove, A. Chekhtman, M. Gibby, G. J. Fishman, S. McBreen, V. L. Chaplin, S. Guiriec, E. Layden, P. N. Bhat, M. Hughes, J. Greiner, A. Kienlin, R. M. Kippen, C. A. Meegan, W. S. Paciesas, R. D. Preece, C. Wilson-Hodge, R. H. Holzworth, and M. L. Hutchins. Terrestrial gamma-ray flashes in the Fermi era: Improved observations and analysis

- methods. *Journal of Geophysical Research (Space Physics)*, 118:3805–3830, June 2013. doi: 10.1002/jgra.50205.
- D. Burlon, G. Ghirlanda, G. Ghisellini, J. Greiner, and A. Celotti. Time resolved spectral behavior of bright BATSE precursors. *A&A*, 505:569–575, October 2009. doi: 10.1051/0004-6361/200912662.
- A. C. Collazzi, C. Kouveliotou, A. J. van der Horst, G. A. Younes, Y. Kaneko, E. Göğüş, L. Lin, J. Granot, M. H. Finger, V. L. Chaplin, D. Huppenkothen, A. L. Watts, A. von Kienlin, M. G. Baring, D. Gruber, P. N. Bhat, M. H. Gibby, N. Gehrels, J. McEnery, M. van der Klis, and R. A. M. J. Wijers. The Five Year Fermi/GBM Magnetar Burst Catalog. *ApJS*, 218:11, May 2015. doi: 10.1088/0067-0049/218/1/11.
- V. Connaughton, M. S. Briggs, A. Goldstein, C. A. Meegan, W. S. Paciesas, R. D. Preece, C. A. Wilson-Hodge, M. H. Gibby, J. Greiner, D. Gruber, P. Jenke, R. M. Kippen, V. Pelassa, S. Xiong, H.-F. Yu, P. N. Bhat, J. M. Burgess, D. Byrne, G. Fitzpatrick, S. Foley, M. M. Giles, S. Guiriec, A. J. van der Horst, A. von Kienlin, S. McBreen, S. McGlynn, D. Tierney, and B.-B. Zhang. Localization of Gamma-Ray Bursts Using the Fermi Gamma-Ray Burst Monitor. *ApJS*, 216:32, February 2015. doi: 10.1088/0067-0049/216/2/32.
- J. R. Dwyer, B. W. Grefenstette, and D. M. Smith. High-energy electron beams launched into space by thunderstorms. *Geophys. Res. Lett.*, 35:L02815, January 2008. doi: 10.1029/2007GL032430.
- C. Ferrigno, Savchenko V., Mereghetti S., Kuulkers E., Bazzano A., Bozzo E., and Courvoisier T. J.-L. LIGO/Virgo G184098: INTEGRAL search of temporally coincident prompt hard X-ray emission. *GRB Coordinates Network*, 18354, 2015.
- B. Giacomazzo, R. Perna, L. Rezzolla, E. Troja, and D. Lazzati. Compact Binary Progenitors of Short Gamma-Ray Bursts. *ApJ*, 762:L18, January 2013. doi: 10.1088/2041-8205/762/2/L18.
- D. Gruber, A. Goldstein, V. Weller von Ahlefeld, P. Narayana Bhat, E. Bissaldi, M. S. Briggs, D. Byrne, W. H. Cleveland, V. Connaughton, R. Diehl, G. J. Fishman, G. Fitzpatrick, S. Foley, M. Gibby, M. M. Giles, J. Greiner, S. Guiriec, A. J. van der Horst, A. von Kienlin, C. Kouveliotou, E. Layden, L. Lin, C. A. Meegan, S. McGlynn, W. S. Paciesas, V. Pelassa, R. D. Preece, A. Rau, C. A. Wilson-Hodge, S. Xiong, G. Younes, and H.-F. Yu. The Fermi GBM Gamma-Ray Burst Spectral Catalog: Four Years of Data. *ApJS*, 211:12, March 2014. doi: 10.1088/0067-0049/211/1/12.
- B. A. Harmon, G. J. Fishman, C. A. Wilson, W. S. Paciesas, S. N. Zhang, M. H. Finger, T. M. Koshut, M. L. McCollough, C. R. Robinson, and B. C. Rubin. The Burst and Transient Source Experiment Earth Occultation Technique. *ApJS*, 138:149–183, January 2002. doi: 10.1086/324018.

- M. L. Hutchins, R. H. Holzworth, J. B. Brundell, and C. J. Rodger. Relative detection efficiency of the World Wide Lightning Location Network. *Radio Science*, 47:RS6005, December 2012. doi: 10.1029/2012RS005049.
- P. Jenke, Linares M., V. Connaughton, E. Beklen, A. Camero-Arranz, , M. H. Finger, and C. A. Wilson-Hodge. The Fermi-GBM 3-year X-ray Burst Catalog. Submitted to *ApJ*.
- L. Z. Kelley, I. Mandel, and E. Ramirez-Ruiz. Electromagnetic transients as triggers in searches for gravitational waves from compact binary mergers. *Phys. Rev. D*, 87(12):123004, June 2013. doi: 10.1103/PhysRevD.87.123004.
- T. M. Koshut, C. Kouveliotou, W. S. Paciesas, J. van Paradijs, G. N. Pendleton, M. S. Briggs, G. J. Fishman, and C. A. Meegan. Gamma-Ray Burst Precursor Activity as Observed with BATSE. *ApJ*, 452:145, October 1995. doi: 10.1086/176286.
- LIGO Scientific Collaboration, J. Aasi, B. P. Abbott, R. Abbott, T. Abbott, M. R. Abernathy, K. Ackley, C. Adams, T. Adams, P. Addesso, and et al. Advanced LIGO. *Classical and Quantum Gravity*, 32(7):074001, April 2015. doi: 10.1088/0264-9381/32/7/074001.
- L. Mayer, S. Kazantzidis, P. Madau, M. Colpi, T. Quinn, and J. Wadsley. Rapid Formation of Supermassive Black Hole Binaries in Galaxy Mergers with Gas. *Science*, 316:1874, June 2007. doi: 10.1126/science.1141858.
- C. Meegan, G. Lichti, P. N. Bhat, E. Bissaldi, M. S. Briggs, V. Connaughton, R. Diehl, G. Fishman, J. Greiner, A. S. Hoover, A. J. van der Horst, A. von Kienlin, R. M. Kippen, C. Kouveliotou, S. McBreen, W. S. Paciesas, R. Preece, H. Steinle, M. S. Wallace, R. B. Wilson, and C. Wilson-Hodge. The Fermi Gamma-ray Burst Monitor. *ApJ*, 702:791–804, September 2009. doi: 10.1088/0004-637X/702/1/791.
- B. D. Metzger, G. Martínez-Pinedo, S. Darbha, E. Quataert, A. Arcones, D. Kasen, R. Thomas, P. Nugent, I. V. Panov, and N. T. Zinner. Electromagnetic counterparts of compact object mergers powered by the radioactive decay of r-process nuclei. *MNRAS*, 406:2650–2662, August 2010. doi: 10.1111/j.1365-2966.2010.16864.x.
- G. N. Pendleton, M. S. Briggs, R. M. Kippen, W. S. Paciesas, M. Stollberg, P. Woods, C. A. Meegan, G. J. Fishman, M. L. McCollough, and V. Connaughton. The Structure and Evolution of LOCBURST: The BATSE Burst Location Algorithm. *ApJ*, 512:362–376, February 1999. doi: 10.1086/306735.
- C. J. Rodger, J. B. Brundell, R. H. Holzworth, and E. H. Lay. Growing detection efficiency of the world wide lightning location network. In N. B. Crosby, T.-Y. Huang, and M. J. Rycroft, editors, *Conf. Proc. 1118, Coupling of Thunderstorms and Lightning Discharges to Near-Earth Space*, pages 15–20. AIP, 2009.

- R. K. Said, U. S. Inan, and K. L. Cummins. Long-range lightning geolocation using a VLF radio atmospheric waveform bank. *Journal of Geophysical Research (Atmospheres)*, 115:D23108, December 2010. doi: 10.1029/2010JD013863.
- R. K. Said, M. B. Cohen, and U. S. Inan. Highly intense lightning over the oceans: Estimated peak currents from global GLD360 observations. *Journal of Geophysical Research (Atmospheres)*, 118:6905–6915, July 2013. doi: 10.1002/jgrd.50508.
- K. Siellez, M. Boër, and B. Gendre. Simultaneous event detection rates by electromagnetic and gravitational wave detectors in the advanced era of LIGO and Virgo. *MNRAS*, 437: 649–655, January 2014. doi: 10.1093/mnras/stt1915.
- N. R. Tanvir, A. J. Levan, A. S. Fruchter, J. Hjorth, R. A. Hounsell, K. Wiersema, and R. L. Tunnicliffe. A ‘kilonova’ associated with the short-duration γ -ray burst GRB 130603B. *Nature*, 500:547–549, August 2013. doi: 10.1038/nature12505.
- The *Fermi*-LAT Collaboration. 2016.
- The LIGO Scientific Collaboration and Virgo. LIGO/Virgo G184098:Burst candidate in LIGO engineering run data. *GRB Coordinates Network*, 18330, 2015a.
- The LIGO Scientific Collaboration and Virgo. LIGO/Virgo G184098: Ongoing gravitational-wave analysis. *GRB Coordinates Network*, 18388, 2015b.
- The LIGO Scientific Collaboration and Virgo. LIGO/Virgo G184098: Updated FAR estimate. *GRB Coordinates Network*, 18851, 2015c.
- The LIGO Scientific Collaboration and Virgo. LIGO/Virgo G184098: Refined localizations from CBC parameter estimation. *GRB Coordinates Network*, 18858, 2015d.
- E. Troja, S. Rosswog, and N. Gehrels. Precursors of Short Gamma-ray Bursts. *ApJ*, 723: 1711–1717, November 2010. doi: 10.1088/0004-637X/723/2/1711.
- A. von Kienlin, C. A. Meegan, W. S. Paciesas, P. N. Bhat, E. Bissaldi, M. S. Briggs, J. M. Burgess, D. Byrne, V. Chaplin, W. Cleveland, V. Connaughton, A. C. Collazzi, G. Fitzpatrick, S. Foley, M. Gibby, M. Giles, A. Goldstein, J. Greiner, D. Gruber, S. Guiriec, A. J. van der Horst, C. Kouveliotou, E. Layden, S. McBreen, S. McGlynn, V. Pelassa, R. D. Preece, A. Rau, D. Tierney, C. A. Wilson-Hodge, S. Xiong, G. Younes, and H.-F. Yu. The Second Fermi GBM Gamma-Ray Burst Catalog: The First Four Years. *ApJS*, 211:13, March 2014. doi: 10.1088/0067-0049/211/1/13.
- D. Wanderman and T. Piran. The rate, luminosity function and time delay of non-Collapsar short GRBs. *MNRAS*, 448:3026–3037, April 2015. doi: 10.1093/mnras/stv123.

C. A. Wilson-Hodge, G. L. Case, M. L. Cherry, J. Rodi, A. Camero-Arranz, P. Jenke, V. Chaplin, E. Beklen, M. Finger, N. Bhat, M. S. Briggs, V. Connaughton, J. Greiner, R. M. Kippen, C. A. Meegan, W. S. Paciasas, R. Preece, and A. von Kienlin. Three Years of Fermi GBM Earth Occultation Monitoring: Observations of Hard X-Ray/Soft Gamma-Ray Sources. *ApJS*, 201:33, August 2012. doi: 10.1088/0067-0049/201/2/33.